

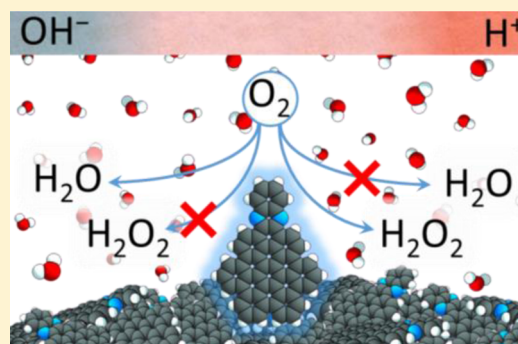
# A Model for the pH-Dependent Selectivity of the Oxygen Reduction Reaction Electrocatalyzed by N-Doped Graphitic Carbon

Benjamin W. Noffke, Qiqi Li, Krishnan Raghavachari,\* and Liang-shi Li\*

Department of Chemistry, Indiana University, Bloomington, Indiana 47405, United States

**S** Supporting Information

**ABSTRACT:** Nitrogen-doped graphitic carbon materials have been extensively studied as potential replacements for Pt-based electrocatalysts for the oxygen reduction reaction (ORR). However, little is known about the catalytic mechanisms, including the parameters that determine the selectivity of the reaction. By comparing theoretical calculations of the ORR selectivity at a well-defined graphene nanostructure with experimental results, we propose a model based on interfacial solvation to explain the observed preference for the four-electron pathway in alkaline electrolytes. The hydrophobic environment around the active sites, as in enzymatic catalysis, restricts the access of water and destabilizes small ionic species such as peroxide, the product of the two-electron pathway. This model, when applied to acidic electrolytes, shows the ORR preferring the two-electron pathway, consistent with the well-known pH-dependent ORR selectivity catalyzed by graphitic carbon materials. Because of the similarity between more complex N-doped graphitic carbon materials and our model system, we can extend this model to the former and rationalize nearly all of the previously reported experimental results on the selectivity of ORR catalyzed by these materials.



## INTRODUCTION

The oxygen reduction reaction (ORR) is a crucial step in devices such as fuel cells to directly convert fuels to electricity at a moderate temperature. Toward the ultimate goal of replacing Pt-based electrocatalysts for the ORR with those made of abundant elements, metal-free, N-doped graphitic carbon materials have been intensively studied as potential alternatives.<sup>1–4</sup> However, the complexity and heterogeneity of these materials have severely hindered mechanistic studies of the catalytic reactions. As a result, many outstanding questions pertaining to the carbon catalysis persist, ranging from the roles of the nitrogen dopants to the sequence of reactions in the catalytic cycle. In particular, there has been little understanding about what determines the ORR selectivity in these materials, as the ORR in an aqueous environment can proceed through either a four-electron (4e) pathway to directly yield H<sub>2</sub>O (or OH<sup>−</sup>), or a two-electron (2e) pathway to produce H<sub>2</sub>O<sub>2</sub>. For ORR electrocatalysts made of metal-free, N-doped graphitic carbon materials, a vast majority of experimental work has shown that an alkaline condition (e.g., pH = 13) appears to be necessary for the 4e-pathway;<sup>5</sup> whereas in acidic electrolytes (e.g., pH = 1) the ORR almost always proceeds through the 2e-pathway.<sup>6–9</sup> Because the 4e-pathway can generate more electric energy with a noncorrosive product H<sub>2</sub>O, it is generally preferred for electricity production. Moreover, to avoid poisoning of the fuel cells by ambient CO<sub>2</sub>, it is desirable that the ORR electrocatalysts be active under acidic conditions.<sup>10</sup> Thus, understanding the ORR selectivity of N-doped graphitic carbon materials has great practical signifi-

cance. Herein by comparing theoretical investigation of heterogeneous ORR electrocatalysts made of well-defined N-doped graphene nanostructures with experimental observations, we show that solvation around the reaction sites is an important parameter determining the selectivity of the electrocatalyzed ORR. This result is generally applicable to more complex N-doped carbon materials, enabling us to propose a model to rationalize previous experimental results on the pH-dependent ORR selectivity at carbon-based electrocatalysts.

A characteristic of heterogeneous electrocatalysts is the presence of liquid–solid interfaces, for which a full description is not yet available.<sup>11,12</sup> In particular, theoretical studies have demonstrated the importance of solvation for various electrocatalyzed reactions at the interfaces.<sup>13–16</sup> Similarly, for the carbon electrocatalysts, water molecules around the reaction sites have been treated either explicitly<sup>17–19</sup> or with continuum solvent models, both assuming that water molecules are freely accessible to the reaction sites. However, most of the graphitic carbon used for catalysis has mesoporous structures and is hydrophobic in nature,<sup>20–22</sup> raising the question whether this is a reasonable assumption. A similar situation occurs in enzyme-catalyzed reactions with active sites buried in hydrophobic interior of the proteins.<sup>23,24</sup> Ionizable groups such as carboxylic acids or amines have their pK<sub>a</sub> values altered by the environment, favoring uncharged states to fulfill catalytic

Received: June 30, 2016

Published: October 13, 2016

functions in various reactions. This was rationalized via limited access of water to the sites due to the hydrophobic local environments, that can be phenomenologically described with a dielectric constant that is much lower (typically 2.5–4)<sup>25</sup> than that of bulk water (i.e., 78).<sup>26–28</sup>

Herein we apply the same phenomenological approach to investigate the effects of solvation at the interfaces on the ORR selectivity. Previously Yeager and co-workers found that a hydrophobic coating on platinum could decrease the ORR overpotential.<sup>29,30</sup> It was attributed to the limited access of water at the hydrophobic interface and the consequent decrease in dielectric constant that favors adsorption of the nonpolar O<sub>2</sub>. Here with well-defined N-doped graphene nanostructures, we show that the lower dielectric constant could greatly influence the selectivity of the ORR. We show that the solvation model can be extended to explain previous experimental results on ORR selectivity electrocatalyzed by more complex N-doped graphitic carbon materials in both basic and acidic conditions.

## METHODS AND COMPUTATIONAL DETAILS

In our calculations, we explicitly study well-defined N-doped colloidal graphene nanostructures<sup>31–33</sup> as a model system for mechanistic studies of graphitic carbon materials. As reported previously, the graphene nanostructures are made with stepwise solution chemistry, and consequently they not only have a uniform size but also contain nitrogen dopants with a uniform bonding configuration. Therefore, these well-defined nanostructures enable us to directly compare theoretical calculations with experimental results without the need for assumptions regarding the size of the conjugated carbon framework or the positions and bonding configurations of the dopants. An example is **1** shown in Figure 1, which contains a phenazine moiety containing nitrogen dopants exclusively in a “pyridinic” configuration.<sup>34</sup> **1** is soluble in common organic solvents but not in water because of the peripheral trialkylphenyl group that makes a cage to prevent aggregation (an energy-minimized geometry in vacuum is shown in

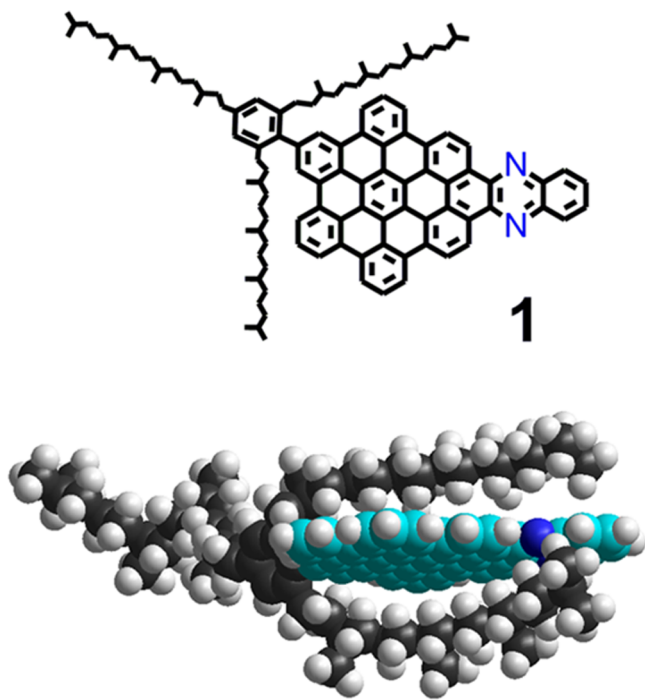


**Figure 1.** Structure of N-doped graphene quantum dot (**1**) (upper) and its space filling model (lower), showing the enclosing nature of solubilizing alkyl chains.

Figure 1, lower).<sup>35,36</sup> As a result, **1** can be readily immobilized on an electrode, forming a solid film in an aqueous environment as a heterogeneous electrocatalyst. Our previous experimental studies have shown that in alkaline solutions (pH = 13) **1** electrocatalyzes the ORR predominantly through the 4e-pathway to produce water.<sup>33</sup> Further, comparing the electrochemical properties of **1** with the ORR onset potential revealed that it is a carbanion intermediate **2** (Figure 2) that

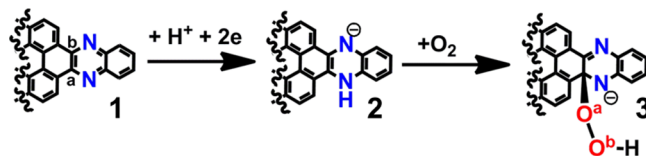


**Figure 2.** Previously reported mechanism of oxygen activation by **1**.<sup>33</sup> **1** undergoes a two-electron, one-proton reduction to form the reactive anion intermediate **2**, which activates oxygen to form peroxygraphene anion **3**. The structures of the species involved are truncated for clarity. In **1** and **3**, the alphabetically labeled carbon and oxygen atoms are for our discussion hereinafter.

activates oxygen. **2** is generated from **1** by a one-proton, two-electron reduction, and subsequently reacts with molecular dioxygen to form a peroxygraphene anion intermediate (**3**).<sup>33</sup> Figure 2 shows the atoms around the site of oxygen binding, that according to our calculations is a carbon atom and we label it as C<sup>a</sup>. For clarity in the discussion hereinafter, we also label important carbon and oxygen atoms in the vicinity as C<sup>b</sup>, O<sup>a</sup>, and O<sup>b</sup>, respectively. Herein we use density functional theory (DFT) calculations to study the fate of **3** because it determines the selectivity of the ORR and will provide other mechanistic insights regarding the catalyzed ORR.

As described in more detail in the Supporting Information (SI), the M06-2X density functional was used in our calculations.<sup>37</sup> Optimized geometries and frequencies (yielding zero-point energies and thermal corrections) were obtained in the gas phase using the 6-31G(d,p) basis set for carbon and hydrogen atoms and the 6-31+G(d,p) basis set for nitrogen and oxygen atoms.<sup>38–43</sup> Solvation corrections to the free energies were obtained with the SMD implicit solvation model<sup>44</sup> with the 6-31+G(d,p) basis set. It has been demonstrated frequently that continuum solvation models provide accurate solution phase thermochemical data for catalytic chemical reactions.<sup>45,46</sup> Thermal and solvation corrections were included in conjunction with gas phase single point energies calculated with the 6-311+G(2df,p) basis set<sup>47</sup> to yield the Gibbs free energies of the species. All calculations were performed with the Gaussian 09 program suite.<sup>48</sup> The robustness of our conclusions is also examined with a different density functional and a different solvation model (the B3LYP density functional<sup>49</sup> with Grimme's D3 corrections<sup>50</sup> and the IEFPCM solvation model,<sup>51–64</sup> see the SI for details). The interaction of the electric field with the dipole moment and polarizability tensor of the involved species was examined, but its contribution was negligible (see the SI for details).

## RESULTS AND DISCUSSION

### Two-Electron vs Four-Electron Pathways at pH = 13.

With DFT calculations, we investigated reactions of peroxygraphene anion **3** (Figure 2). Our calculations showed that either C–O or O–O bond cleavage could occur, thus revealing the branching point for the 2e and 4e-pathways. Shown in Figure 3 are the calculated transition state of O–O bond cleavage (**4**) in the gas phase that leads the reaction down the 4e-pathway and its product (**5**). The transition state **4** involves oxygen atom O<sup>a</sup> bridging over to a neighboring carbon atom C<sup>b</sup> and the O<sup>a</sup>–O<sup>b</sup> bond cleavage. This leads to **5** in which C<sup>a</sup>–C<sup>b</sup> bond breaks and the O<sup>b</sup>H group forms a new bond with C<sup>a</sup>. The reaction has an activation barrier of 1.60 eV and a free energy change of –1.41 eV. Despite its high activation barrier, it is highly irreversible and, once occurs, ensures the reaction to

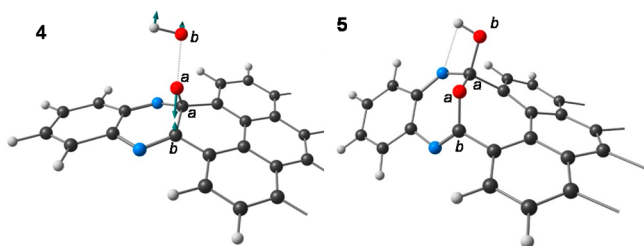


**Figure 3.** Transition state (4) for O–O bond cleavage and the resultant intermediate (5). In 4, the arrows indicate the displacement vectors of the normal mode leading to O–O bond cleavage.

continue through the 4e-pathway. The resultant intermediate 5 is somewhat peculiar. It nevertheless is similar to a structure previously reported in fullerene  $C_{60}$  derivatives,<sup>65,66</sup> where a bridging oxygen atom takes the place of a C–C single bond.

In the gas phase, the C–O bond cleavage is thermodynamically unfavorable by +1.30 eV and there is no stationary point on the potential energy surface corresponding to a transition state. The product is found to be **1** recovered accompanied by the release of  $HO_2^-$  at infinite separation. The source of this instability is due to the electrostatic penalty of the C–O bond cleavage in the gas phase. A delocalized negative charge on a large molecular system being replaced with one localized on a much smaller peroxide anion (thermodynamically favored over neutral  $H_2O_2$  at pH = 13) is electrostatically unfavorable. This clearly indicates the necessity of including solvation in understanding the ORR catalyzed by carbon materials.

To account for solvation in the ORR, we first assumed an environment with a dielectric constant  $\epsilon = 78$  and compare the results with those for  $\epsilon = 1$  (in gas phase) at pH = 13. **Figure 4**

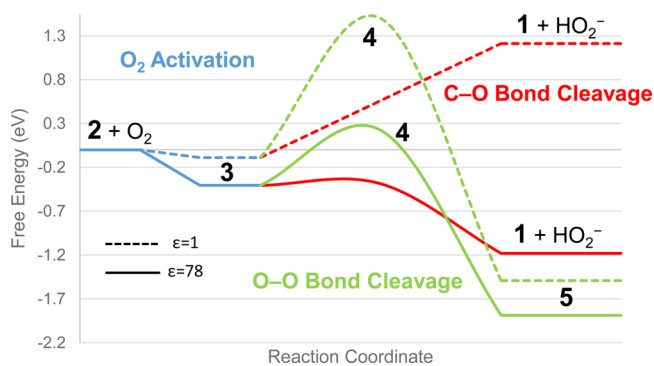


**Figure 4.** Free energy diagram of the branching point for 2e- and 4e-selectivity of ORR at pH = 13 in **3** solvated with implicit water with a dielectric constant  $\epsilon$  of 78 (solid lines) and the gas phase ( $\epsilon = 1$ , dotted lines). The blue line represents oxygen activation, the green line O–O bond cleavage, and the red line C–O bond cleavage. Labels in bold text refer to molecule labels that appear **Figures 2** and **3**. All energy values are relative to  $2 + O_2$  (g, 1 atm).

shows the calculated reaction free energy changes and free energy barriers of the 2e and 4e-pathways at  $\epsilon = 78$  and 1, respectively. In the figure, the blue line represents the oxygen activation step observed experimentally at  $-0.40$  V (vs SCE), the green line represents O–O bond cleavage or the 4e-pathway, and the red line represents C–O bond cleavage or the 2e-pathway. Text in bold refers to molecule labels in **Figures 1** and **2**, and all energies are relative to  $2 + O_2$  (g, 1 atm). Qualitatively the 4e-pathway is similar between  $\epsilon = 78$  and 1. Solvated with an implicit model at a dielectric constant of 78,

the free energy activation barrier is 0.63 eV and free energy change is  $-1.48$  eV (in contrast to 1.60 and  $-1.41$  eV, respectively for  $\epsilon = 1$ ). The activation barrier turns out to be quite sensitive to the solvation conditions, differing by nearly a factor of 2. The reaction free energy change is not affected significantly. Thus, the O–O bond cleavage remains thermodynamically favorable over a wide range of dielectric constant.

For the 2e-pathway, the dielectric constant is a parameter sufficiently important to determine whether the reaction occurs or not. Because in the standard protocol of the SMD model<sup>44</sup> the geometry optimizations are done in the gas phase, that reveals no transition state for C–O bond cleavage, we carried out the geometry optimizations with implicit solvation to obtain the potential energy surface (see the SI for more details). For a dielectric constant of 78, we found that the reaction barrier for the C–O bond cleavage is almost nonexistent (0.04 eV) and the reaction free energy is  $-0.78$  eV. The nonexistent barrier suggests that the C–O bond cleavage should be highly favored kinetically over the O–O bond cleavage (with a barrier of 0.63 eV). As a result, the 2e-pathway should be preferred at pH = 13, that, however, contradicts our experimental results that the 4e-selectivity is the predominant pathway.<sup>33</sup>

The calculated lower activation barrier for the 2e-pathway than the 4e-pathway can be understood with the molecular orbitals of peroxygraphene anion **3**. **Figure 5** shows the

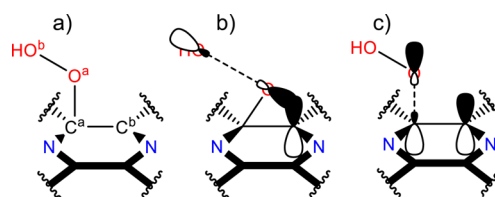


**Figure 5.** Illustrative frontier molecular orbitals to explain kinetics of 4e and 2e-transition states. (a) Truncated version of **3** for reference. (b) O–O bond cleavage transition state that shows O–O  $\sigma^*$  orbital, which overlaps with the neighboring  $\pi$  orbital of the carbon atom. (c) C–O bond cleavage transition state that shows C–O  $\sigma^*$  orbital, which can overlap with the neighboring  $\pi$  orbitals of the nitrogen and carbon atom.

geometry of **3** around the nitrogen dopants, as well as the frontier molecular orbitals responsible for the bond cleavages. **Figure 5b** shows the unoccupied O–O  $\sigma^*$  orbital and the occupied  $\pi$  orbital on the neighboring carbon atom, that interact to cause the O–O bond cleavage. The higher energy of the O–O  $\sigma^*$  orbital, along with the need for bending the O–C<sup>a</sup>–C<sup>b</sup> angle, results in a higher activation barrier for the O–O bond cleavage. The O–O bond cleavage resembles an  $S_N2$  reaction, where carbon atom C<sup>b</sup> acts as a nucleophile, oxygen atom O<sup>a</sup> acts as an electrophile, and  $OH^-$  as a leaving group which however is captured by carbon atom C<sup>a</sup>. The 4e-pathway is not sensitive to the solvation environment because of the migration of the OH group to carbon atom C<sup>a</sup> to form **4** with no release of  $OH^-$ . **Figure 5c** shows the unoccupied C–O  $\sigma^*$  orbital and the occupied  $\pi$  orbital of the neighboring carbon atom, that interact to initiate the C–O bond cleavage. This process resembles an E1cB-elimination reaction,<sup>67</sup> with  $HO_2^-$  eliminated and a C=C bond formed. The low lying C–O  $\sigma^*$  orbital makes the C–O bond cleavage facile. However, the release of the  $HO_2^-$  anion is heavily dependent on the dielectric

environment, being thermodynamically favored in a high- $\epsilon$  environment but not when  $\epsilon$  is small.

**Dielectric-Constant Dependence of ORR Selectivity at pH = 13.** The discrepancy between our experiments on ORR selectivity and our calculated results, assuming the reaction to be water-solvated ( $\epsilon = 78$ ), naturally raises the question whether it is a valid assumption. Our experimental results showed a predominant 4e-pathway yet our calculations favor the 2e-pathway. With well-known examples set by enzyme-catalyzed reactions with active sites buried in hydrophobic interior,<sup>68</sup> this discrepancy is hardly surprising considering the apolar alkyl groups encompassing the conjugated core in **1** (Figure 1). In a solid film of **1** used in the electrocatalytic studies, as in the hydrophobic interior of the enzymes, the alkyl groups effectively provide a similar environment that limits access of water molecules to the active sites. A similar effect has also been documented for a platinum surface coated with a hydrophobic additive that leads to decreased ORR overpotential.<sup>29,30</sup> This may be phenomenologically described with a dielectric constant much smaller than 78, as in the case of enzymes wherein  $\epsilon < 10$  (typically 2.5–4) is generally accepted.<sup>25,27,69</sup> Thus, we examined how the two ORR pathways are affected by varying the  $\epsilon$  values within the framework of the continuum solvation model.

Figure 6 shows how the reaction free energies and free energy barriers change when the dielectric constant  $\epsilon$  varies

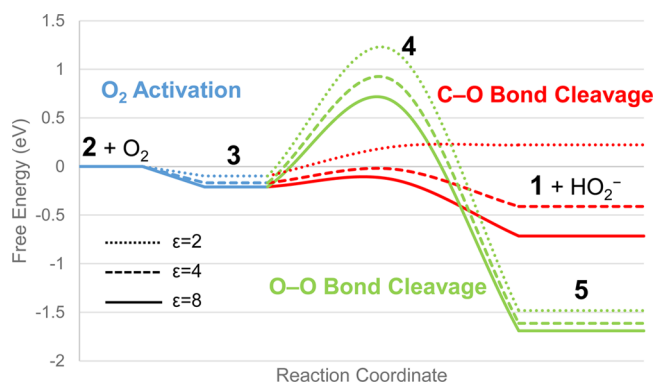


**Figure 6.** Free energy diagram of branching point for 2e- and 4e-selectivity of ORR at pH = 13 in **3** solvated with implicit water with a dielectric constant  $\epsilon$  of 8 (solid lines), 4 (dashed lines), and 2 (dotted lines). The blue line represents oxygen activation, the green line represents O–O bond cleavage, and the red line represents C–O bond cleavage. Labels in bold text refer to molecule labels that appear in Figures 2 and 3. All energies are relative to **2** + O<sub>2</sub> (g, 1 atm).

between 8 and 2, that are in the range of commonly accepted values (i.e., smaller than 10) for enzymatic reactions.<sup>70–72</sup> With a dielectric constant of 8 (or 2), the values for the activation barrier and free energy change of the O–O bond cleavage shift to +0.88 (or +1.30) eV and –1.48 (or –1.38) eV, respectively. The activation barrier is sensitive to the dielectric constant, while the reaction driving force is practically independent of the permittivity of the medium. The 4e-pathway is thermodynamically insensitive to the dielectric constant because the formation of **5** does not involve the release of a small ionic species. Thus, the O–O bond cleavage can proceed with the charge delocalized on the graphitic core of the catalyst. In contrast, the reaction free energy change for the C–O bond cleavage at dielectric constants of 8 and 2 are –0.51 eV and +0.32 eV, respectively. Thus, the 2e-pathway is much more sensitive to

the dielectric constant of the surrounding medium than the 4e-pathway, which has serious implications for the ORR selectivity. At the expected dielectric constant value for this environment,  $\epsilon < 10$ , the 2e-pathway could be thermodynamically unfavorable at an interpolated value of 2.6 (see SI for details). The dielectric constant threshold at which release of HO<sub>2</sub><sup>-</sup> becomes unfavorable is subject to change within the error of the calculation (see Figure S3 in SI), which is estimated to be 0.25 eV (see Table S1 in the SI). This leads to an approximate range of 2.1–4.1 for the dielectric constant, comparable to previously reported range for folded proteins.<sup>25</sup> This is due to the electrostatic penalty associated with localizing a charge from a larger graphene system to the much smaller peroxide anion in low dielectric medium at pH = 13. Thus, at low dielectric constants, the 2e-pathway is thermodynamically unfavorable, leaving the 4e-pathway, though slow, as the only option at this pH value.

The calculated threshold dielectric constant at which the 2e-pathway turns unfavorable does not depend on the functional and solvation model used. Combinations of M06-2X and B3LYP with the two solvation models, SMD and IEFPCM (see Figure S4 in the SI), produce a threshold dielectric constant close to the range of 2.1–4.1 (see Table S2 in the SI).

**Two-Electron vs Four-Electron Pathways in Acidic Media.** Within the framework of the dielectric-constant-dependent ORR selectivity, we anticipate that the pH value of the electrolyte solution can significantly modify the ORR selectivity. In particular, in acidic media (e.g., pH = 1) it is the neutral hydrogen peroxide H<sub>2</sub>O<sub>2</sub> (pK<sub>a</sub> = 11.74) that is the thermodynamically stable product of the 2e-pathway rather than the peroxide anion we discussed for pH = 13. Neutral H<sub>2</sub>O<sub>2</sub> has drastically different solvation energy from the anion, and thus different dielectric constant dependence can be anticipated. However, experimentally we found that **1** has no appreciable ORR activity in acidic media. We have attributed this to more rapid protonation of **2** resulting in a product that is not capable of activating oxygen.<sup>33</sup> Nevertheless, some of more complex N-doped carbon materials have been shown to catalyze the ORR at pH = 1, and peroxygraphene intermediates like **3** have been proposed consisting of an oxygen molecule chemisorbed to a carbon atom adjacent to a nitrogen dopant.<sup>73–83</sup> Therefore, despite being inaccessible in the particular catalytic system we study, peroxygraphene intermediate like **3** appears to be universal to N-doped carbon catalysts for the ORR. Hence we study the fate of **3** in acidic media and we believe work of this kind can provide instructive insights regarding the ORR selectivity in acidic media.

The protonated form of **3** at pH = 1 is shown as **6** in Figure 7. Our calculations show that the nitrogen atom adjacent to the oxygen binding carbon atom (C<sup>a</sup>) is more basic because of intramolecular hydrogen bonding with O<sup>a</sup>. From **6**, H<sub>2</sub>O<sub>2</sub> can be eliminated by going through transition state **7**, in which the C<sup>a</sup>–O<sup>a</sup> bond breaks and hydrogen transfers to the peroxy group, as shown by the arrows in the figure marking the displacement vectors corresponding the transition state normal mode. Transition state **8** corresponds to O–O bond cleavage at pH = 1 and resembles transition state **4** at pH = 13. The arrows in Figure 7 show that the O–O bond is broken and the proton approaches the liberated hydroxyl group. The resulting O–O bond cleavage intermediate is altered by the presence of a proton in that the hydroxyl group can leave as H<sub>2</sub>O, forming intermediate **9** instead of **5**.

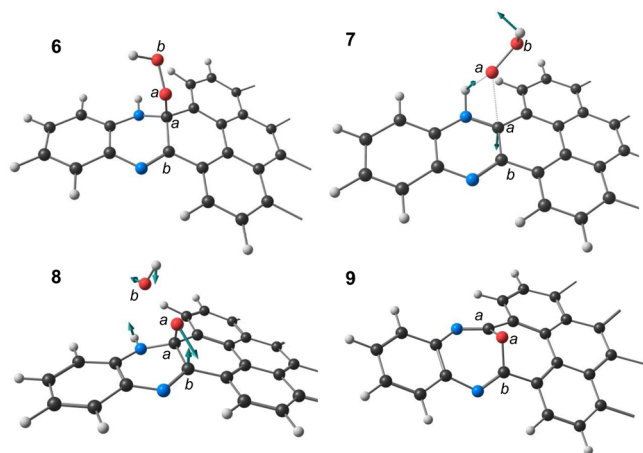


**Figure 7.** Intermediates and transition states in acidic conditions. Protonated form of **3** (**6**), transition state for hydrogen peroxide elimination (**7**), transition state for water production via O–O bond cleavage (**8**), and the oxygen-bridged intermediate resulting from O–O bond cleavage (**9**). Arrows in **7** and **8** indicate the displacement vectors of the normal modes responsible for H<sub>2</sub>O<sub>2</sub> elimination and H<sub>2</sub>O production, respectively.

**Figure 8** shows the calculated free energy diagrams when protonation is considered in the 4e and 2e-pathways at pH = 1

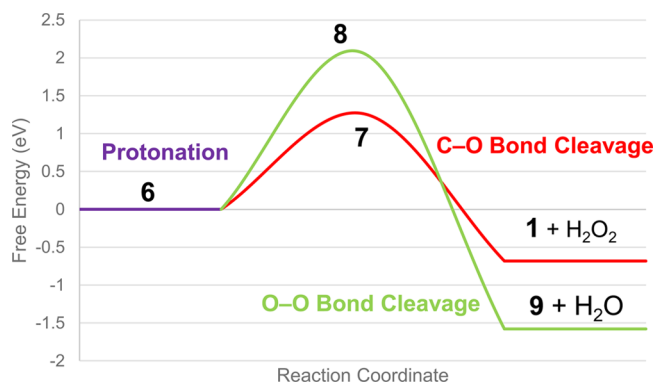


**Figure 8.** Free energy diagram of branching point for 2e- and 4e-selectivity of ORR in **3** with implicit solvation with a dielectric constant of 4 at pH = 1. The blue line represents oxygen activation, the green line represents the O–O bond cleavage for the 4e-pathway, the red line represents the C–O bond cleavage for the 2e-pathway at pH = 1. Labels in bold text refer to molecule labels that appear **Figures 2** and **7**. All energies are relative to pure solid **6**.

and  $\epsilon = 4$ . O–O bond cleavage from **6** to yield **9** and H<sub>2</sub>O has a barrier of +2.06 eV and is favored by –1.58 eV. H<sub>2</sub>O<sub>2</sub>-elimination has an activation barrier of +1.27 eV and a driving force of –0.68 eV, which is kinetically favored considerably over the 4e-pathway, supporting selectivity for the 2e-pathway in acidic conditions. The protonation of **3** to generate **6** mitigates the issue of the low dielectric surroundings, allowing the 2e-pathway through elimination of H<sub>2</sub>O<sub>2</sub>. The electrostatic penalty of localizing the charge onto HO<sub>2</sub><sup>–</sup> in a low permittivity environment is circumvented through neutralizing the system with a proton. The relative positions of the O–O and C–O  $\sigma^*$  orbitals indicate that when both the 4e and 2e-pathways products are thermodynamically favorable, the 2e-pathway will be kinetically preferred.

### The Solvation Model Extended to More Complex N-Doped Carbon Materials.

Our calculations show that the dielectric constant influences the ORR selectivity largely because solvation affects thermodynamics of the 2e-pathway, which is applicable to the ORR electrocatalyzed by any N-doped carbon material. Previous studies on more complex carbon materials supported the peroxygraphene as a key intermediate.<sup>73–83</sup> Thus, our results on **3** are of general significance to explain the selectivity of the metal-free graphitic carbon catalysts. Porous carbon materials used in catalysis, unless treated with surfactants, are well-known for their hydrophobicity and poor wettability by water.<sup>20–22</sup> Therefore, the question we raised regarding the solvation at the interface remains broadly relevant. In addition, it is generally accepted that the dielectric constant of an electrode surface is significantly smaller due to the rigidly aligned water molecules at the interface.<sup>84</sup> Therefore, the limited access of water molecules and ordered water structures at the electrode surfaces severely limit the solvation of HO<sub>2</sub><sup>–</sup> and in turn lead to selectivity for the 4e-pathway in alkaline media. This is consistent with the vast majority of previous reported experimental work that alkaline conditions appear to be necessary for the ORR to proceed through the 4e-pathway.

For the N-doped carbon ORR catalysts that are active in acidic conditions,<sup>6,9</sup> our model can successfully explain the observed preference for the 2e-pathway. As in the case of **1**, the pH-dependence of the ORR selectivity can be understood with the stability of the neutral H<sub>2</sub>O<sub>2</sub> over the HO<sub>2</sub><sup>–</sup> anion due to protonation. With protons readily available, the 2e-pathway may proceed through H<sub>2</sub>O<sub>2</sub> elimination, which is thermodynamically allowed by the low dielectric constant of the surroundings. Despite the large driving force of the 4e-pathway, the 2e-pathway has a much lower activation barrier, which is rooted in the frontier molecular orbitals of the peroxygraphene intermediate, and thus is considerably faster and kinetically preferred.

We have also investigated the dielectric constant dependence of the alkaline 2e-pathway for a single pyridine nitrogen and graphitic nitrogen functionalities to survey the extension of our model to other nitrogen functionalities. These additional nitrogen functionalities show the same trend of unfavorable release of HO<sub>2</sub><sup>–</sup> when the dielectric constant decreases (more details in the **SI**, **Figure S5** and **Table S3**). Pyrrolic nitrogen is not considered in our studies because it is not stable at high temperatures during synthesis,<sup>85–87</sup> where it is reported to turn into pyridinic and graphitic nitrogen during annealing. It is also reported that pyrrolic nitrogen sites are less active than pyridinic sites for catalyzing the ORR,<sup>88</sup> while it is generally believed that pyridinic and graphitic nitrogen sites are responsible for ORR activity.<sup>73,89–91</sup>

It has been reported that the 2e-pathway can be dominant in some related systems even in alkaline conditions,<sup>92,93</sup> which can also be understood with our model. All such N-doped carbon catalysts were shown to be rich in oxygen because the precursors to the catalysts often contain oxygen atoms or oxygen is present in the synthesis.<sup>94</sup> The oxygen dopants often result in acidic sites, such as carboxylic acids, anhydrides, lactones, or phenols, in the heterogeneous system, that make possible sources of protons. Thus, we speculate that such acidic groups in N-doped carbon catalysts may alter the kinetics and thermodynamics of H<sub>2</sub>O<sub>2</sub> elimination even in alkaline electrolytes. A proton from a proximal acidic oxygen-containing group can assist C–O bond cleavage, changing the product from

$\text{HO}_2^-$  to  $\text{H}_2\text{O}_2$  and mitigating the effect of the decreased local dielectric constant. There have been many such examples in enzymatic reactions and homogeneous catalytic systems. A well-known example is proton shuttling in, e.g., carbonic anhydrase or GTP synthase, in which a local acidic group (a protonated histidine residue or a tyrosine residue) donates a proton to facilitate a bond cleavage.<sup>95–97</sup> Similarly, in the oxygen-rich carbon materials, the peroxygraphene intermediate may accept a proton from the acidic sites associated with oxygen dopants and, like **3** in acidic conditions, facilitate the C–O bond cleavage. Similarly, introducing a phenol group to the ligand of a metal-centered  $\text{CO}_2$  reduction catalyst was found to influence the reactivity of the catalyst via the acidic proton of the phenol group.<sup>98,99</sup>

There have also been occasional reports that in acid electrolytes, the ORR electrocatalyzed by N-doped carbon materials proceeds through the 4e-pathway.<sup>100–103</sup> This pathway is particularly important when the carbon materials are mesoporous, and the formation of  $\text{H}_2\text{O}$  has been attributed to further reduction of trapped  $\text{H}_2\text{O}_2$  generated through the 2e-pathway.<sup>6</sup> Extraordinarily high porosity of these materials causes poor mass transport, leading to the reduction of the trapped  $\text{H}_2\text{O}_2$  being faster than its diffusion away from the catalyst. The authors noted that modifying the morphology of the catalyst and improving the mass transport of the system shifted the selectivity to the 2e-pathway. The trapping of  $\text{H}_2\text{O}_2$  has also been shown to depend on catalyst loading in the measurements, where reduced loadings were shown to shift the selectivity to the 2e-pathway.<sup>104</sup> Our experimental study on **1** has shown that its ORR selectivity is independent of the catalyst loading (see the SI), and thus the trapping of  $\text{H}_2\text{O}_2$  followed by further reduction cannot explain the observed 4e-pathway.

## SUMMARY

In summary, in this work, we have proposed a model based on solvation around the active sites to understand selectivity of the ORR catalyzed by N-doped graphitic carbon. The model was calibrated by comparing theoretical calculations of a well-defined graphene nanostructure with experimental results, and is able to provide a general understanding of the pH-dependent ORR selectivity catalyzed by nearly all of the previously reported graphitic carbon materials. Overall, while our approach is able to explain the key experimental observations including the pH-dependence, it still has the limitation of modeling the effective dielectric constant in a phenomenological manner. Additionally, we have treated the solvation effects using a continuum model without having explicit solvent interactions. A fully molecular level quantum mechanical description of the entire surface–system interactions including explicit solvation effects is computationally prohibitive currently, though it would clearly be desirable in the future.

## ASSOCIATED CONTENT

### Supporting Information

The Supporting Information is available free of charge on the ACS Publications website at DOI: 10.1021/jacs.6b06778.

Details of the calculation scheme, evaluation of error, auxiliary structural considerations, and molecular coordinates (PDF)

## AUTHOR INFORMATION

### Corresponding Authors

\*kraghava@indiana.edu

\*li23@indiana.edu

### Notes

The authors declare no competing financial interest.

## ACKNOWLEDGMENTS

We acknowledge NSF (DMR-1105185, CBET-1610712) and DOE (Grant No. DE-FG02-07ER15889) for financial support. This research was supported in part by Lilly Endowment, Inc., through its support for the Indiana University Pervasive Technology Institute, and in part by the Indiana METACyt Initiative.

## REFERENCES

- (1) Greeley, J.; Stephens, I. E. L.; Bondarenko, A. S.; Johansson, T. P.; Hansen, H. A.; Jaramillo, T. F.; Rossmeisl, J.; Chorkendorff, I.; Nørskov, J. K. *Nat. Chem.* **2009**, *1*, 552.
- (2) Gewirth, A. A.; Thorum, M. S. *Inorg. Chem.* **2010**, *49*, 3557.
- (3) Yu, D.; Nagelli, E.; Du, F.; Dai, L. *J. Phys. Chem. Lett.* **2010**, *1*, 2165.
- (4) Wu, G.; Zelenay, P. *Acc. Chem. Res.* **2013**, *46*, 1878.
- (5) Dai, L.; Xue, Y.; Qu, L.; Choi, H.-J.; Baek, J.-B. *Chem. Rev.* **2015**, *115*, 4823.
- (6) Park, J.; Nabaie, Y.; Hayakawa, T.; Kakimoto, M.-a. *ACS Catal.* **2014**, *4*, 3749.
- (7) Iwazaki, T.; Obinata, R.; Sugimoto, W.; Takasu, Y. *Electrochem. Commun.* **2009**, *11*, 376.
- (8) Wei, W.; Liang, H.; Parvez, K.; Zhuang, X.; Feng, X.; Müllen, K. *Angew. Chem., Int. Ed.* **2014**, *53*, 1570.
- (9) Bai, J. C.; Zhu, Q. Q.; Lv, Z. X.; Dong, H. Z.; Yu, J. H.; Dong, L. *Int. J. Hydrogen Energy* **2013**, *38*, 1413.
- (10) Steele, B. C.; Heinzel, A. *Nature* **2001**, *414*, 345.
- (11) Jahn, M.; Gekle, S. *Phys. Rev. E* **2015**, *92*, 052130.
- (12) Akiyama, R.; Hirata, F. *J. Chem. Phys.* **1998**, *108*, 4904.
- (13) Sha, Y.; Yu, T. H.; Liu, Y.; Merinov, B. V.; Goddard, W. A., III. *J. Phys. Chem. Lett.* **2010**, *1*, 856.
- (14) Wieckowski, A.; Neurock, M. *Adv. Phys. Chem.* **2011**, *2011*, 907129.
- (15) Hamada, I.; Morikawa, Y. *J. Phys. Chem. C* **2008**, *112*, 10889.
- (16) Okamoto, Y.; Sugino, O.; Mochizuki, Y.; Ikeshoji, T.; Morikawa, Y. *Chem. Phys. Lett.* **2003**, *377*, 236.
- (17) Okamoto, Y. *Appl. Surf. Sci.* **2009**, *256*, 335.
- (18) Yu, L.; Pan, X.; Cao, X.; Hu, P.; Bao, X. *J. Catal.* **2011**, *282*, 183.
- (19) Chai, G.; Hou, Z.; Shu, D.; Ikeda, T.; Terakura, K. *J. Am. Chem. Soc.* **2014**, *136*, 13629.
- (20) Ahnert, F.; Arafat, H. A.; Pinto, N. G. *Adsorption* **2003**, *9*, 311.
- (21) Boehm, H. P. *Carbon* **1994**, *32*, 759.
- (22) Groszek, A. J.; Partyka, S. *Langmuir* **1993**, *9*, 2721.
- (23) Harris, T. K.; Turner, G. J. *IUBMB Life* **2002**, *53*, 85.
- (24) Schutz, C. N.; Warshel, A. *Proteins: Struct., Funct., Genet.* **2001**, *44*, 400.
- (25) Gilson, M. K.; Honig, B. H. *Biopolymers* **1986**, *25*, 2097.
- (26) Löffler, G.; Schreiber, H.; Steinhäuser, O. *J. Mol. Biol.* **1997**, *270*, 520.
- (27) Simonson, T.; Perahia, D. *Proc. Natl. Acad. Sci. U. S. A.* **1995**, *92*, 1082.
- (28) Smith, P. E.; Brunne, R. M.; Mark, A. E.; Van Gunsteren, W. F. *J. Phys. Chem.* **1993**, *97*, 2009.
- (29) Yeager, E.; Razaq, M.; Gervasio, D.; Razaq, A.; Tryk, D. *Proc. Workshop Struct. Eff. Electrocatal. Oxygen Electrochem.* **1993**, *92*, 440.
- (30) Razaq, M.; Razaq, A.; Yeager, E.; DesMarteau, D. D.; Singh, S. J. *Electrochem. Soc.* **1989**, *136*, 385.
- (31) Yan, X.; Li, B.; Li, L.-S. *Acc. Chem. Res.* **2013**, *46*, 2254.
- (32) Li, Q.; Noffke, B. W.; Liu, Y.; Li, L.-S. *Curr. Opin. Colloid Interface Sci.* **2015**, *20*, 346.

- (33) Li, Q.; Noffke, B. W.; Wang, Y.; Menezes, B.; Peters, D. G.; Raghavachari, K.; Li, L.-s. *J. Am. Chem. Soc.* **2014**, *136*, 3358.
- (34) Li, Q.; Zhang, S.; Dai, L.; Li, L.-s. *J. Am. Chem. Soc.* **2012**, *134*, 18932.
- (35) Yan, X.; Cui, X.; Li, B.; Li, L.-s. *Nano Lett.* **2010**, *10*, 1869.
- (36) Yan, X.; Li, L.-S. *J. Mater. Chem.* **2011**, *21*, 3295.
- (37) Zhao, Y.; Truhlar, D. *Theor. Chem. Acc.* **2008**, *120*, 215.
- (38) Ditchfield, R.; Hehre, W. J.; Pople, J. A. *J. Chem. Phys.* **1971**, *54*, 724.
- (39) Hehre, W. J.; Ditchfield, R.; Pople, J. A. *J. Chem. Phys.* **1972**, *56*, 2257.
- (40) Hariharan, P. C.; Pople, J. A. *Theoret. Chim. Acta* **1973**, *28*, 213.
- (41) Hariharan, P. C.; Pople, J. A. *Mol. Phys.* **1974**, *27*, 209.
- (42) Gordon, M. S. *Chem. Phys. Lett.* **1980**, *76*, 163.
- (43) Francl, M. M.; Pietro, W. J.; Hehre, W. J.; Binkley, J. S.; Gordon, M. S.; DeFrees, D. J.; Pople, J. A. *J. Chem. Phys.* **1982**, *77*, 3654.
- (44) Marenich, A. V.; Cramer, C. J.; Truhlar, D. G. *J. Phys. Chem. B* **2009**, *113*, 6378.
- (45) Solis, B. H.; Hammes-Schiffer, S. *Inorg. Chem.* **2011**, *50*, 11252.
- (46) Varela-Álvarez, A.; Yang, T.; Jennings, H.; Kornecki, K. P.; Macmillan, S. N.; Lancaster, K. M.; Mack, J. B. C.; Du Bois, J.; Berry, J. F.; Musaev, D. G. *J. Am. Chem. Soc.* **2016**, *138*, 2327.
- (47) Krishnan, R.; Binkley, J. S.; Seeger, R.; Pople, J. A. *J. Chem. Phys.* **1980**, *72*, 650.
- (48) Frisch, M. J.; Trucks, G. W.; Schlegel, H. B.; Scuseria, G. E.; Robb, M. A.; Cheeseman, J. R.; Scalmani, G.; Barone, V.; Mennucci, B.; Petersson, G. A.; Nakatsuji, H.; Caricato, M.; Li, X.; Hratchian, H. P.; Izmaylov, A. F.; Bloino, J.; Zheng, G.; Sonnenberg, J. L.; Hada, M.; Ehara, M.; Toyota, K.; Fukuda, R.; Hasegawa, J.; Ishida, M.; Nakajima, T.; Honda, Y.; Kitao, O.; Nakai, H.; Vreven, T.; Montgomery, J. A., Jr.; Peralta, J. E.; Ogliaro, F.; Bearpark, M. J.; Heyd, J.; Brothers, E. N.; Kudin, K. N.; Staroverov, V. N.; Kobayashi, R.; Normand, J.; Raghavachari, K.; Rendell, A. P.; Burant, J. C.; Iyengar, S. S.; Tomasi, J.; Cossi, M.; Rega, N.; Millam, N. J.; Klene, M.; Knox, J. E.; Cross, J. B.; Bakken, V.; Adamo, C.; Jaramillo, J.; Gomperts, R.; Stratmann, R. E.; Yazyev, O.; Austin, A. J.; Cammi, R.; Pomelli, C.; Ochterski, J. W.; Martin, R. L.; Morokuma, K.; Zakrzewski, V. G.; Voth, G. A.; Salvador, P.; Dannenberg, J. J.; Dapprich, S.; Daniels, A. D.; Farkas, Ö.; Foresman, J. B.; Ortiz, J. V.; Cioslowski, J.; Fox, D. J. *Gaussian 09*; Gaussian, Inc.: Wallingford, CT, 2009.
- (49) Becke, A. D. *J. Chem. Phys.* **1993**, *98*, 5648.
- (50) Grimme, S.; Antony, J.; Ehrlich, S.; Krieg, H. *J. Chem. Phys.* **2010**, *132*, 154104.
- (51) Barone, V.; Cossi, M. *J. Phys. Chem. A* **1998**, *102*, 1995.
- (52) Barone, V.; Cossi, M.; Tomasi, J. *J. Chem. Phys.* **1997**, *107*, 3210.
- (53) Barone, V.; Cossi, M.; Tomasi, J. *J. Comput. Chem.* **1998**, *19*, 404.
- (54) Cancès, E.; Mennucci, B.; Tomasi, J. *J. Chem. Phys.* **1997**, *107*, 3032.
- (55) Cossi, M.; Barone, V.; Cammi, R.; Tomasi, J. *Chem. Phys. Lett.* **1996**, *255*, 327.
- (56) Cossi, M.; Barone, V.; Mennucci, B.; Tomasi, J. *Chem. Phys. Lett.* **1998**, *286*, 253.
- (57) Cossi, M.; Rega, N.; Scalmani, G.; Barone, V. *J. Chem. Phys.* **2001**, *114*, 5691.
- (58) Cossi, M.; Scalmani, G.; Rega, N.; Barone, V. *J. Chem. Phys.* **2002**, *117*, 43.
- (59) Mennucci, B.; Cancès, E.; Tomasi, J. *J. Phys. Chem. B* **1997**, *101*, 10506.
- (60) Mennucci, B.; Tomasi, J. *J. Chem. Phys.* **1997**, *106*, 5151.
- (61) Miertus, S.; Scrocco, E.; Tomasi, J. *Chem. Phys.* **1981**, *55*, 117.
- (62) Miertus, S.; Tomasi, J. *Chem. Phys.* **1982**, *65*, 239.
- (63) Pascual-ahuir, J. L.; Silla, E.; Tuñón, I. *J. Comput. Chem.* **1994**, *15*, 1127.
- (64) Tomasi, J.; Mennucci, B.; Cancès, E. *J. Mol. Struct.: THEOCHEM* **1999**, *464*, 211.
- (65) Raghavachari, K. *Chem. Phys. Lett.* **1992**, *195*, 221.
- (66) Raghavachari, K. *Int. J. Mod. Phys. B* **1992**, *6*, 3821.
- (67) Gronert, S. *J. Am. Chem. Soc.* **1992**, *114*, 2349.
- (68) Fahmy, K.; Sakmar, T. P.; Siebert, F. *Biochemistry* **2000**, *39*, 10607.
- (69) García-Moreno, B. E.; Dwyer, J. J.; Gittis, A. G.; Lattman, E. E.; Spencer, D. S.; Stites, W. E. *Biophys. Chem.* **1997**, *64*, 211.
- (70) Harvey, S. C.; Hoekstra, P. *J. Phys. Chem.* **1972**, *76*, 2987.
- (71) Bone, S.; Pethig, R. *J. Mol. Biol.* **1982**, *157*, 571.
- (72) Bone, S.; Pethig, R. *J. Mol. Biol.* **1985**, *181*, 323.
- (73) Saidi, W. A. *J. Phys. Chem. Lett.* **2013**, *4*, 4160.
- (74) Studt, F. *Catal. Lett.* **2013**, *143*, 58.
- (75) Yu, L.; Pan, X.; Cao, X.; Hu, P.; Bao, X. *J. Catal.* **2011**, *282*, 183.
- (76) Vazquez-Arenas, J.; Galano, A.; Lee, D. U.; Higgins, D.; Guevara-García, A.; Chen, Z. *J. Mater. Chem. A* **2016**, *4*, 976.
- (77) Sidik, R. A.; Anderson, A. B.; Subramanian, N. P.; Kumaraguru, S. P.; Popov, B. N. *J. Phys. Chem. B* **2006**, *110*, 1787.
- (78) Fan, X.; Zheng, W. T.; Kuo, J.-L. *RSC Adv.* **2013**, *3*, 5498.
- (79) Kwak, D.; Khetan, A.; Noh, S.; Pitsch, H.; Han, B. *ChemCatChem* **2014**, *6*, 2662.
- (80) Ikeda, T.; Hou, Z.; Chai, G.-L.; Terakura, K. *J. Phys. Chem. C* **2014**, *118*, 17616.
- (81) Ikeda, T.; Boero, M.; Huang, S.-F.; Terakura, K.; Oshima, M.; Ozaki, J.-i. *J. Phys. Chem. C* **2008**, *112*, 14706.
- (82) Jiao, Y.; Zheng, Y.; Jaroniec, M.; Qiao, S. Z. *J. Am. Chem. Soc.* **2014**, *136*, 4394.
- (83) Zhang, P.; Lian, J. S.; Jiang, Q. *Phys. Chem. Chem. Phys.* **2012**, *14*, 11715.
- (84) *Modern Electrochemistry An Introduction to an Interdisciplinary Area*; Bockris, J. O. M., Reddy, A. K. N., Eds.; Springer US: Boston, MA, 1973; Vol 2.
- (85) Sharifi, T.; Hu, G.; Jia, X. E.; Wagberg, T. *ACS Nano* **2012**, *6*, 8904.
- (86) Roy, S. S.; Papakonstantinou, P.; Okpalugo, T. I. T.; Murphy, H. *J. Appl. Phys.* **2006**, *100*, 053703.
- (87) Stanczyk, K.; Dziembaj, R.; Piwowska, Z.; Witkowski, S. *Carbon* **1995**, *33*, 1383.
- (88) Kundu, S.; Nagaiah, T. C.; Xia, W.; Wang, Y. M.; Van Dommele, S.; Bitter, J. H.; Santa, M.; Grundmeier, G.; Bron, M.; Schuhmann, W.; Muhler, M. *J. Phys. Chem. C* **2009**, *113*, 14302.
- (89) Niwa, H.; Horiba, K.; Harada, Y.; Oshima, M.; Ikeda, T.; Terakura, K.; Ozaki, J.-i.; Miyata, S. *J. Power Sources* **2009**, *187*, 93.
- (90) Rao, C. V.; Cabrera, C. R.; Ishikawa, Y. *J. Phys. Chem. Lett.* **2010**, *1*, 2622.
- (91) Lai, L.; Potts, J. R.; Zhan, D.; Wang, L.; Poh, C. K.; Tang, C.; Gong, H.; Shen, Z.; Lin, J.; Ruoff, R. S. *Energy Environ. Sci.* **2012**, *5*, 7936.
- (92) Fukushima, T.; Drisdell, W.; Yano, J.; Surendranath, Y. *J. Am. Chem. Soc.* **2015**, *137*, 10926.
- (93) Wang, Z.; Jia, R.; Zheng, J.; Zhao, J.; Li, L.; Song, J.; Zhu, Z. *ACS Nano* **2011**, *5*, 1677.
- (94) Figueiredo, J. L.; Pereira, M. F. R., Eds. *Carbon Materials for Catalysis*; John Wiley & Sons, Inc.: Hoboken, NJ, 2008; p 177.
- (95) Hubatsch, I.; Mannervik, B. *Biochem. Biophys. Res. Commun.* **2001**, *280*, 878.
- (96) Roitzsch, M.; Fedorova, O.; Pyle, A. M. *Nat. Chem. Biol.* **2010**, *6*, 218.
- (97) Wu, R.; Wang, S.; Zhou, N.; Cao, Z.; Zhang, Y. *J. Am. Chem. Soc.* **2010**, *132*, 9471.
- (98) Agarwal, J.; Shaw, T. W.; Schaefer, H. F.; Bocarsly, A. B. *Inorg. Chem.* **2015**, *54*, 5285.
- (99) Costentin, C.; Passard, G.; Robert, M.; Savéant, J.-M. *J. Am. Chem. Soc.* **2014**, *136*, 11821.
- (100) Shui, J.; Wang, M.; Du, F.; Dai, L. *Sci. Adv.* **2015**, *1*, e1400129.
- (101) Yu, D.; Zhang, Q.; Dai, L. *J. Am. Chem. Soc.* **2010**, *132*, 15127.
- (102) Ding, W.; Wei, Z.; Chen, S.; Qi, X.; Yang, T.; Hu, J.; Wang, D.; Wan, L.-J.; Alvi, S. F.; Li, L. *Angew. Chem., Int. Ed.* **2013**, *52*, 11755.
- (103) Maldonado, S.; Stevenson, K. J. *J. Phys. Chem. B* **2005**, *109*, 4707.
- (104) Bonakdarpour, A.; Lefevre, M.; Yang, R.; Jaouen, F.; Dahn, T.; Dodelet, J.-P.; Dahn, J. *Electrochem. Solid-State Lett.* **2008**, *11*, B105.